Hindawi
International Journal of RF and Microwave Computer-Aided Engineering
Volume 2023, Article ID 5527842, 14 pages
https://doi.org/10.1155/2023/5527842

Research Article

Systematic Analysis of Rotated Dual-Split Elliptical SRR with Band-Stop Characteristics

Swarnadipto Ghosh,[1] **Dipankar Saha**,[1] **Ayona Chakraborty**,[2] **Samik Chakraborty**,[3] **and Bhaskar Gupta**[2]

[1]*Indian Institute of Space Science and Technology, Thiruvananthapuram, India*
[2]*Jadavpur University, Kolkata, India*
[3]*Regent Education and Research Foundation, Kolkata, India*

Correspondence should be addressed to Swarnadipto Ghosh; swarnadipto.2000@gmail.com

Received 7 June 2023; Revised 23 October 2023; Accepted 6 November 2023; Published 28 November 2023

Academic Editor: Yen-Sheng Chen

In this research article, a novel double-split elliptical split ring resonator (DS-ESRR) is proposed to achieve frequency-notching behavior of ultrawideband filtenna, where the semimajor and minor axes of the ellipse are taken as a bivariate random variable and expressed in Ramanujan's correction coefficient so that more degree of freedom is available for choosing degenerated impedance and thus for variable frequency-notching applications. To verify this hypothetical method, finite sets of variables for DS-ESRR are presented in this proposed work, and a mathematical expression is formulated to estimate the resonant frequency of the DS-ESRR, such that for practical applications, frequency-notching parameters can be easily estimated accurately rather than previously used SRR like circular or square-shaped geometry. DS-ESRR is deployed at the back of a CPW-fed ultrawideband antenna for notching filter application, and the computed data is compared with the eigen mode simulation results which reveal good agreement with each other.

1. Introduction

Split ring resonators (SRR) having various structural geometries have been extensively studied and implemented in different interesting electromagnetic and communication applications by different research groups across the globe [1–5] since they were originally proposed [1] in 1999. Most of the applications of SRRs reveal their usefulness to realize the practicality of double negative (DNG) metamaterial and as one of the integral subsystems of narrow and wideband microwave filters, novel compact phase shifters, etc. A unique advantage of using an SRR for such an application is that, as it is a subwavelength structure, the size of these structures is very compact at resonance [6]. For all such applications, the proper calculation and formulation for estimating the resonant frequency of the SRR become very important [7–10].

This article presents an appropriate mathematical closed-form expression for the resonance frequency calculation of the elliptical and double-split elliptical SRRs (DS-ESRR) and examines the effect of the relative angular rotation of the rings of the double-split elliptical SRR on its resonance. A CPW-baked DS-ESRR-loaded ultrawideband (UWB) filtenna is proposed for a strong frequency notching application.

The rest of the article is discussed as follows: Section 2 provides the theoretical background and calculation steps of the resonance frequency of the ESRR and DS-ESRR and the rotational effect of the rings of the SRR. Section 3 reveals the design description of the proposed DSRR-loaded CPW-fed ultrawideband antenna. Section 4 includes the result, discussion, and observations, and concludes the article.

2. Theoretical Analysis of E-SRR and DS-ESRR

Figures 1(a) and 1(b) reveal the schematic diagrams of elliptical and double-split elliptical split ring resonators, respectively. The rings are designed on the top of a substrate having the relative permittivity, ε_r, and dielectric height of

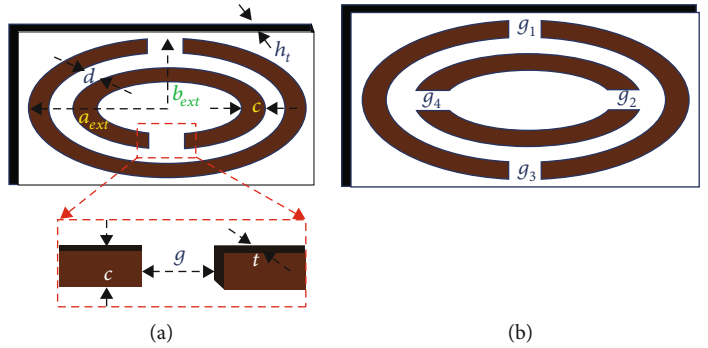

FIGURE 1: Schematic diagram of the proposed (a) ESRR and (b) DS-ESRR.

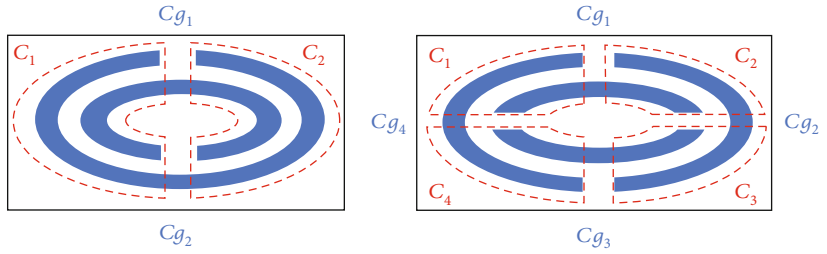

FIGURE 2: (a) Visualization of the realizable capacitances in ESRR and (b) visualization of realizable capacitances in DS-ESRR.

h_t backed by the ground metallic plate on the other side. The other design parameters are as follows: a_{ext} and b_{ext} are the semimajor and semiminor axes of the external elliptical ring, c is the ring width, d is the gap between the outer and inner elliptical ring, and g is the gap width of the two splits facing opposite to each other. In Figure 1(b), the four split widths of double-split elliptical SRR are taken as g_1, g_2, g_3, and g_4, where we usually consider $g_1 = g_2 = g_3 = g_4 = g$.

2.1. Accurate Calculation of Equivalent Capacitance. Single and dual-split ESRR and its cross-section are shown in Figure 2. The proper calculation of the realizable equivalent capacitance is very important to estimate the resonance frequency of the SRR. To obtain the ring capacitance, we take C_{pul} times the average ring length $(\pi(a_{\text{avg}} + b_{\text{avg}}))$, where C_{pul} is the distributed capacitance per unit length. C_{pul}, a_{avg}, and b_{avg} can be expressed as

$$a_{\text{avg}} = a_{\text{ext}} - c - \frac{d}{2},$$
$$b_{\text{avg}} = b_{\text{ext}} - c - \frac{d}{2}, \tag{1}$$

$$C_{\text{pul}} = \frac{\sqrt{\varepsilon_e}}{c_0 Z_0}. \tag{2}$$

Figure 3 shows a schematic diagram of an ellipse having the semimajor axis a_{avg} and semiminor axis b_{avg}.

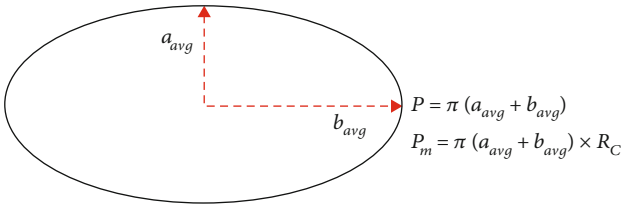

FIGURE 3: Schematic of an elliptical geometry to estimate the perimeter.

The commonly used formula for estimating the perimeter of any ellipse is

$$P = \pi\left(a_{\text{avg}} + b_{\text{avg}}\right), \tag{3}$$

where P is the perimeter of the ellipse and a_{avg} and b_{avg} are the semimajor and semiminor axes of the ellipse, respectively.

But equation (1) is a round-off approximation formula for the perimeter calculation which may cause a significant error in high-frequency applications. As a result, Ramanujan's correction factor has been introduced along with it to calculate the perimeter more accurately using equation (2).

$$P_m = \pi\left(a_{\text{avg}} + b_{\text{avg}}\right)R_C, \tag{4}$$

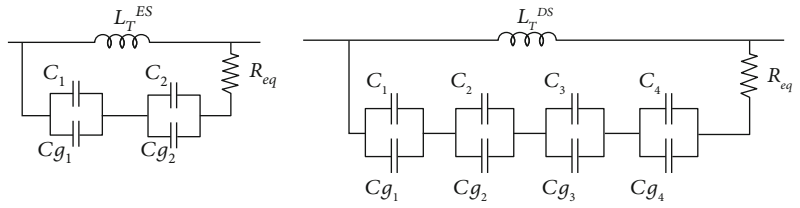

(a) (b)

Figure 4: (a, b) Equivalent circuital realization of the ESRR and DS-ESRR.

Table 1: Resonance frequency calculation for DS-ESRR.

a_{ext} (mm)	b_{ext} (mm)	c (mm)	d (mm)	g (mm)	Freq. (calculated)	Freq. (eigen mode)	Error (%)
8.5	6	0.5	0.7	0.7	4.66	4.30	8.3
5.5	3	0.5	0.8	0.6	8.11	8.36	1.6
6	3	0.5	0.7	0.3	7.34	7.5	2.1
6	2.5	0.4	0.6	0.8	7.18	7.76	2.4
4	2.5	0.4	0.6	0.5	11.30	10.82	4.4
3.5	1.9	0.4	0.5	0.6	13.12	12.44	5.05
3	1.8	0.3	0.6	0.6	14.2	14.12	0.5

where P_m and R_c are the modified perimeter formula and Ramanujan's correction factor, respectively.

$$R_C = \left(1 + \frac{3h}{10 + \sqrt{4 - 3h}}\right), \tag{5}$$

$$h = \frac{\left(a_{\text{avg}} - b_{\text{avg}}\right)^2}{\left(a_{\text{avg}} + b_{\text{avg}}\right)^2}. \tag{6}$$

Hence,

$$P_m = \left[\pi\left(a_{\text{avg}} + b_{\text{avg}}\right) - g\right]\left(1 + \frac{3h}{10 + \sqrt{4 - 3h}}\right). \tag{7}$$

The equivalent distributed capacitance for ESRR and DS-ESRR can be expressed as

$$C^{\text{ESRR}} = \frac{\left[\pi\left(a_{\text{avg}} + b_{\text{avg}}\right) - g\right]C_{\text{pul}}}{2}\left(1 + \frac{3h}{10 + \sqrt{4 - 3h}}\right), \tag{8}$$

$$C^{\text{DS-ESRR}} = \frac{\left[\pi\left(a_{\text{avg}} + b_{\text{avg}}\right) - g\right]C_{\text{pul}}}{4}\left(1 + \frac{3h}{10 + \sqrt{4 - 3h}}\right). \tag{9}$$

Hence, $C^{\text{DS-ESRR}} = C^{\text{ESRR}}/2$.

And the gap capacitance (C_g) experienced between the splits can be derived as

$$C_g = \frac{\varepsilon_0 t}{g}. \tag{10}$$

Table 2: Design parameters of the proposed antenna.

Parameters	Values (mm)	Parameters	Values (mm)
R	1.2	d	0.6
s	0.5	h_t	1.524
w	5	a_{ext}	1.7
c	0.5	b_{ext}	2

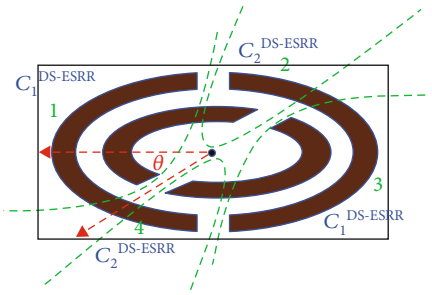

Figure 5: Visualization of realizable capacitances in DS-ESRR.

Hence, the equivalent capacitance expression for ESRR is

$$C_{\text{eq}}^{\text{ESRR}} = \frac{\left(C^{\text{ESRR}} + C_g\right)}{2}. \tag{11}$$

And the equivalent capacitance expression for DS-ESRR can be written as

$$C_{\text{eq}}^{\text{DS-ESRR}} = \frac{\left(C^{\text{DS-ESRR}} + C_g\right)}{4}. \tag{12}$$

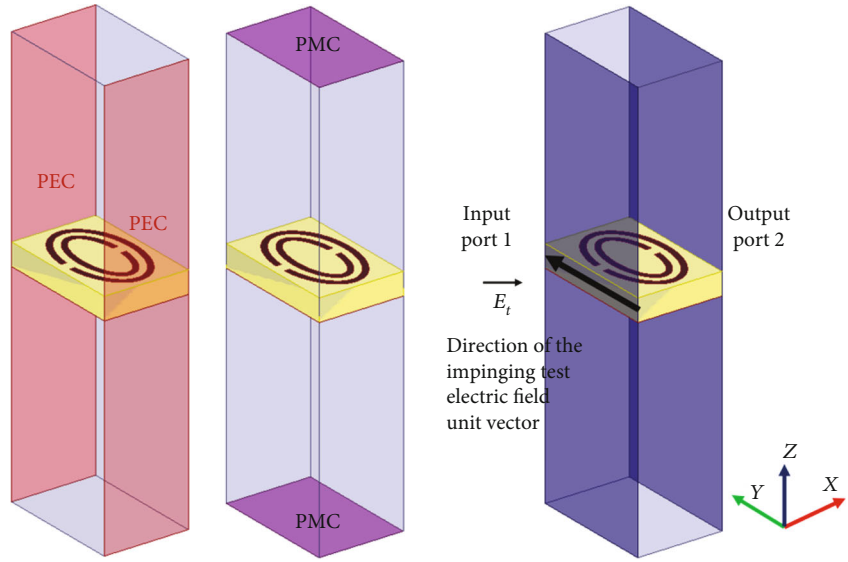

FIGURE 6: Schematic diagram of the proposed elliptical SRR with the essential boundary conditions setup.

2.2. Resonant Frequency Calculation. Figures 4(a) and 4(b) are the equivalent circuital realization of the ESRR and DS-ESRR, respectively. As shown in Figure 4, the expressions for resonance frequencies for ESRR and DS-ESRR can be written

$$\omega_0 = \frac{1}{\sqrt{L_T C_{\text{eq}}}}. \tag{13}$$

The expression of the resonant frequencies of different SRRs is given as

For E-SRR:

$$f_0^{\text{ESRR}} = \frac{1}{2\pi\sqrt{L_T^{ES}\left\{\left[\pi\left(a_{\text{avg}}+b_{\text{avg}}\right)-g\right]C_{\text{pul}}/4\left(1+\left(3h/10+\sqrt{4-3h}\right)\right)+\varepsilon_0 t/2g\right\}}}. \tag{14}$$

For DS-ESRR:

$$f_0^{\text{DS-ESRR}} = \frac{1}{2\pi\sqrt{L_T^{DS}\left\{\left[\pi\left(a_{\text{avg}}+b_{\text{avg}}\right)-g\right]C_{\text{pul}}/16\left(1+\left(3h/10+\sqrt{4-3h}\right)\right)+\varepsilon_0 t/4g\right\}}} \tag{15}$$

From equation (14) and (15), we can conclude that

$$f_0^{\text{ESRR}} = \frac{f_0^{\text{DS-ESRR}}}{2}, \tag{16}$$

where L_T^{ES} and L_T^{DS} are the equivalent distributed inductances of the ESRR and DS-ESRR, respectively.

The general expression for the equivalent distributed inductance is given as

$$L_T = 0.0002l\left(\frac{4l}{c}-\theta\right) \quad nH, \tag{17}$$

where l and c are the length and width of the metallic ring shape and $\theta = 2.451$ for the elliptical shape.

For ESRR:

$$l^{\text{ESRR}} = \pi\left(a_{\text{ext}}+b_{\text{ext}}\right)\left(1+\frac{3h}{10+\sqrt{4-3h}}\right)-g. \tag{18}$$

For DS-ESRR:

$$l^{\text{DS-ESRR}} = \pi\left(a_{\text{ext}}+b_{\text{ext}}\right)\left(1+\frac{3h}{10+\sqrt{4-3h}}\right)-g. \tag{19}$$

The resonance frequencies of the E-SRR are calculated using equations (14) and (15), respectively, for different parameters and compared with the eigen mode simulation results in Tables 1 and 2.

2.3. Rotation Effect on Resonance Frequency. As shown in Figure 5, the length of the sections (1, 3) and (2, 4) can be expressed as P_{m1} and P_{m2}, respectively, through the following (equations (20) and (21)), respectively.

$$P_{m1} = \frac{\left[(\pi+\theta)\left(a_{\text{avg}}+b_{\text{avg}}\right)\right]}{4}Rc, \tag{20}$$

$$P_{m2} = \frac{\left[(\pi-\theta)\left(a_{\text{avg}}+b_{\text{avg}}\right)\right]}{4}Rc. \tag{21}$$

The equivalent distributed capacitance for each section of the rotated DS-ESRR can be written in equations (22) and (23), respectively, as

$$C_1^{\text{DS-ESRR}} = \frac{\left[(\pi+\theta)\left(a_{\text{avg}}+b_{\text{avg}}\right)-g\right]R_C C_{\text{pul}}}{4}, \tag{22}$$

$$C_2^{\text{DS-ESRR}} = \frac{\left[(\pi-\theta)\left(a_{\text{avg}}+b_{\text{avg}}\right)-g\right]R_C C_{\text{pul}}}{4}. \tag{23}$$

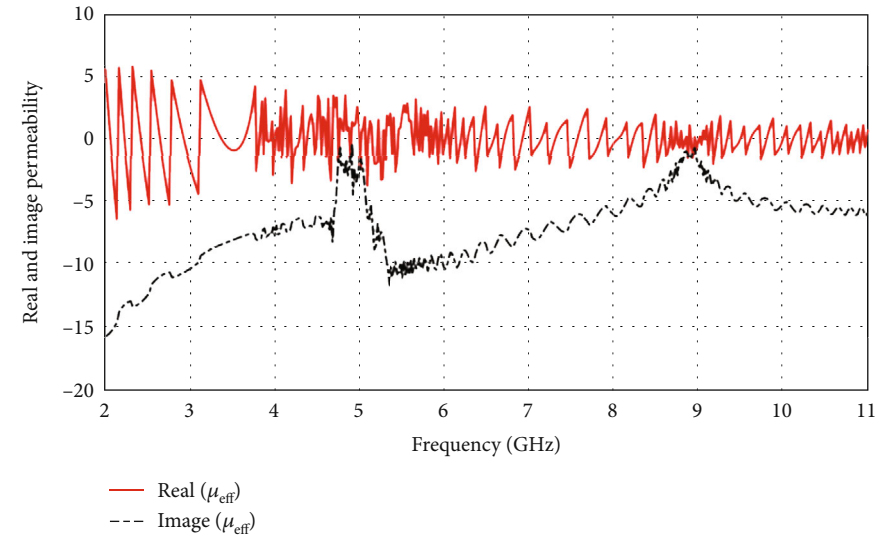

(a)

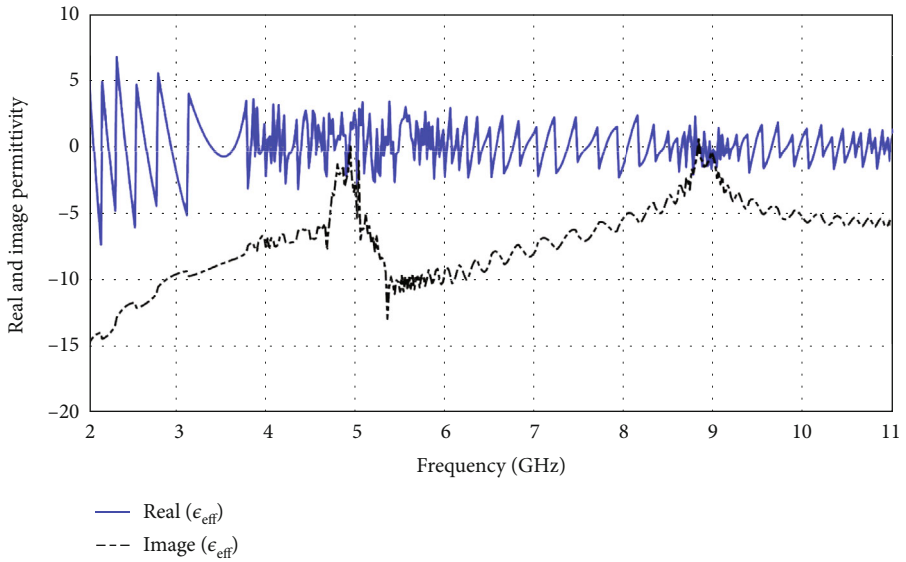

(b)

Figure 7: Continued.

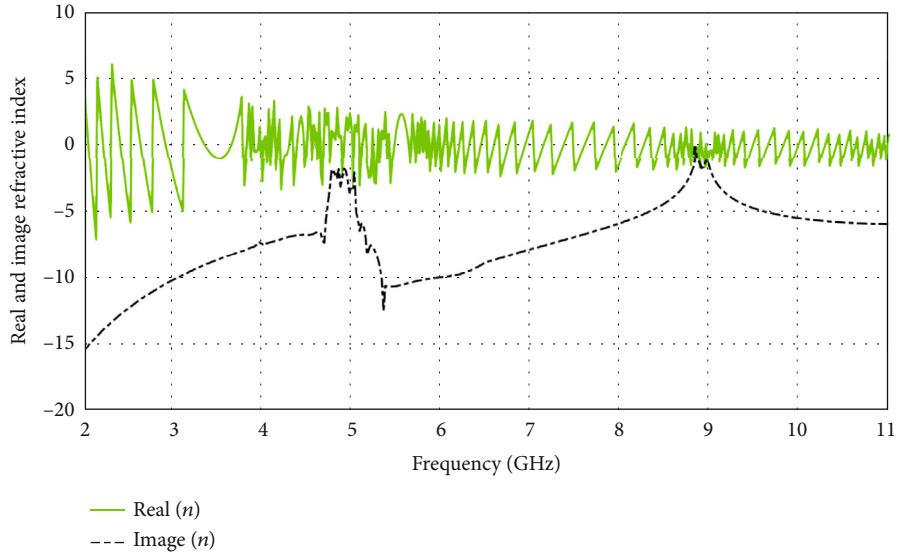

(c)

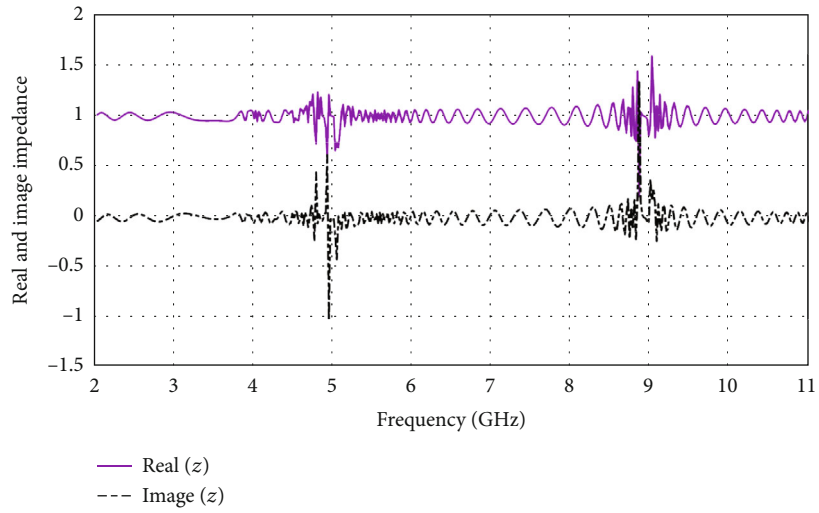

(d)

FIGURE 7: Estimated (a) effective permeability, (b) effective permittivity, (c) effective refractive index, and (d) effective impedance of the proposed elliptical split ring resonator (E-SRR).

And the equivalent capacitance expression for DS-ESRR can be written as

$$C_r^{\text{DS-ESRR}} = \frac{\left(C_1^{\text{DS-ESRR}} + C_g\right)\left(C_2^{\text{DS-ESRR}} + C_g\right)}{2\left(C_1^{\text{DS-ESRR}} + C_2^{\text{DS-ESRR}} + 2C_g\right)}, \tag{24}$$

Substituting $C_1^{\text{DS-ESRR }R}$ and $C_2^{\text{DS-ESRR}}$ from equations (22) and (23), respectively, the simplified $C_r^{\text{DS-ESRR }R}$ can be expressed as

$$C_r^{\text{DS-ESRR}} = \frac{(\pi + x)^2 - \theta^2}{4(\pi + x)}\left[\frac{\left(a_{\text{avg}} + b_{\text{avg}}\right)R_c C_{\text{pul}}}{4}\right], \tag{25}$$

where $x = 4C_g/(a_{\text{avg}} + b_{\text{avg}})R_c C_{\text{pul}}$.

The equivalent capacitance expression for DS-ESRR can be written as

$$C_{\text{req}}^{\text{DS-ESRR}} = \frac{\left(C_r^{\text{DS-ESRR}} + C_g\right)}{4}. \tag{26}$$

As the C_g term is very mall, it can be neglected, and the expression of the resonant frequencies of rotational DS-ESRR is given as

For DS-ESRR:

$$f_{r0}^{\text{DS-ESRR}} = \frac{1}{2\pi\sqrt{L_T\left\{(\pi + x)^2 - \theta^2/4(\pi + x)\left[\left(a_{\text{avg}} + b_{\text{avg}}\right)R_c C_{\text{pul}}/16\right]R_c\right\}}}. \tag{27}$$

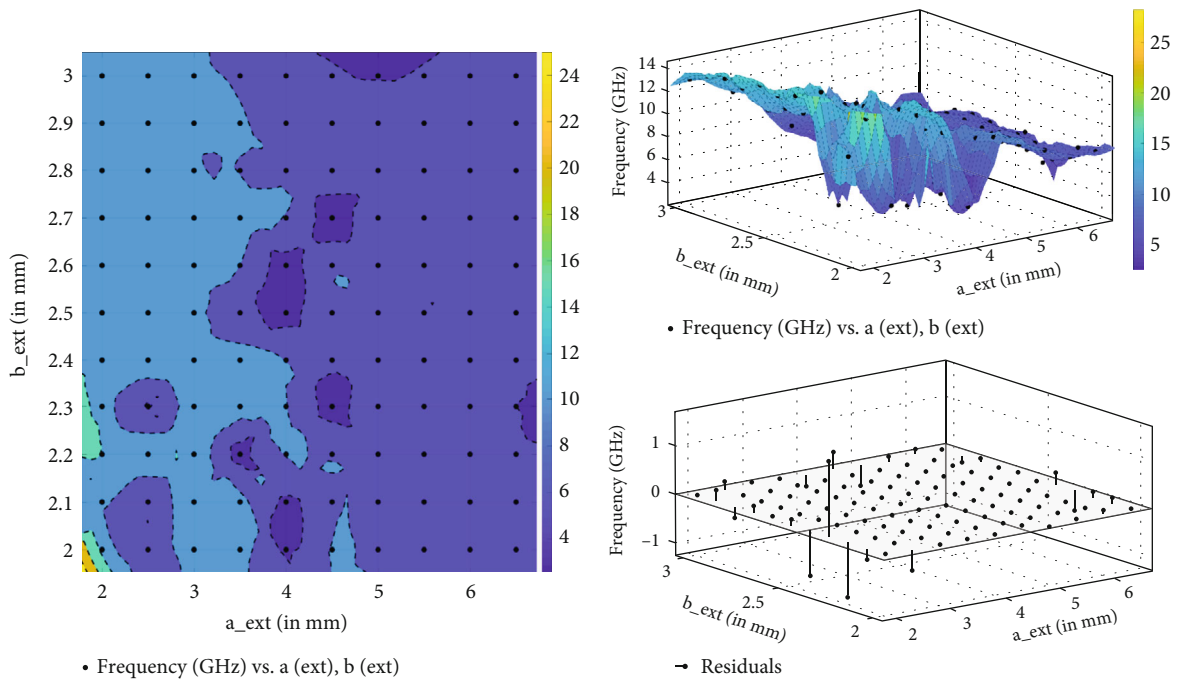

• Frequency (GHz) vs. a (ext), b (ext)

• Frequency (GHz) vs. a (ext), b (ext)

→ Residuals

FIGURE 8: Contour plots and residuals for each (a_{ext}, b_{ext}, and f_0) basis vector mapping.

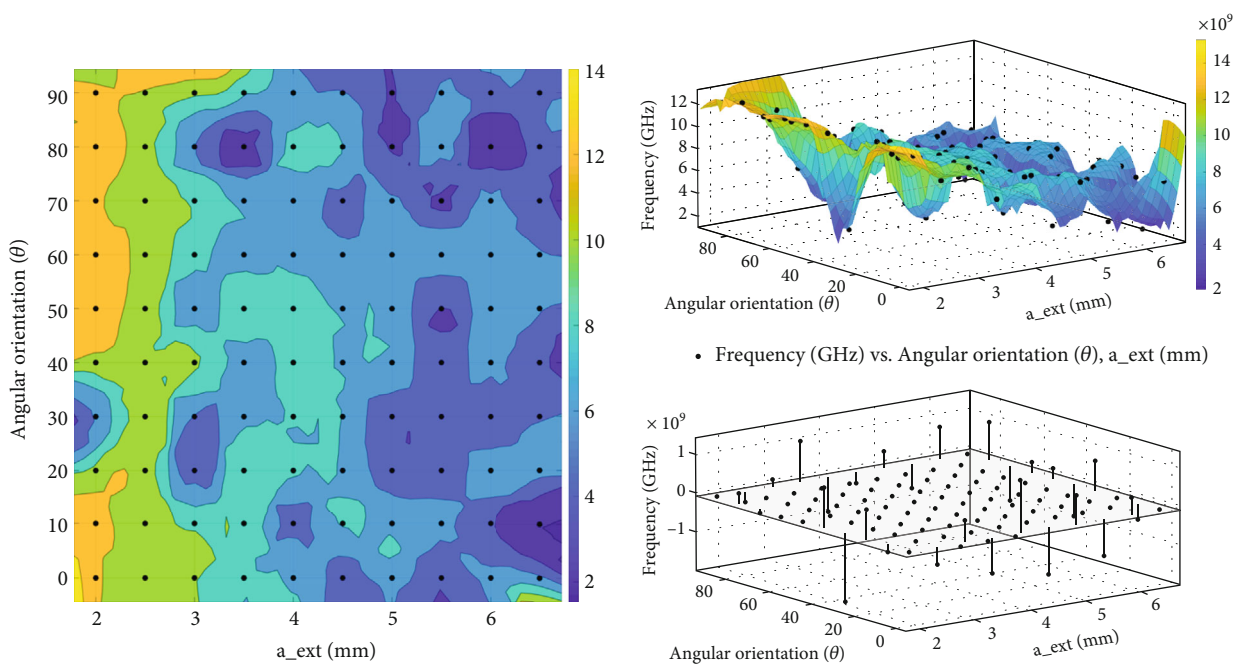

• Frequency (GHz) vs. a_ext (mm), Angular orientation (θ)

• Frequency (GHz) vs. Angular orientation (θ), a_ext (mm)

→ Residuals

FIGURE 9: Contour plots and residuals for each (a_{ext}, θ, and f_0) basis vector mapping.

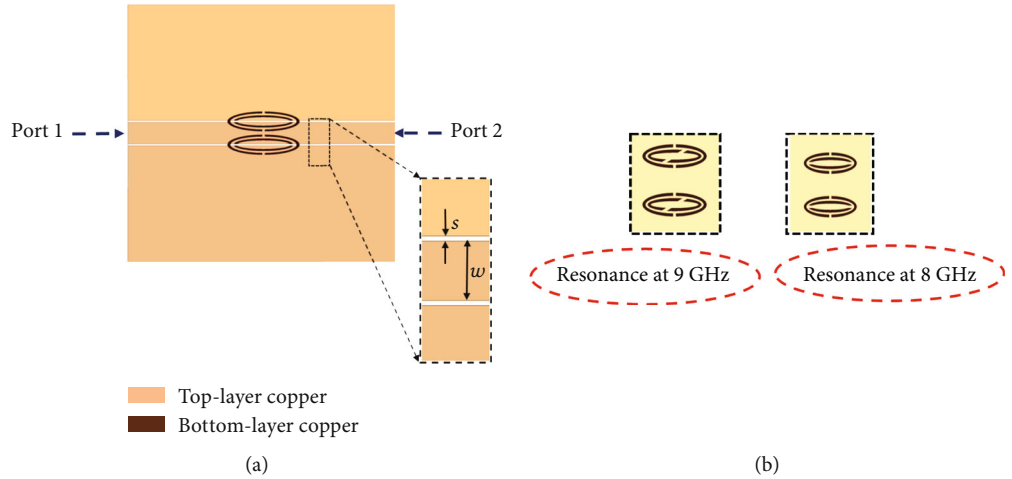

FIGURE 10: (a) Schematic diagram of DS-ESRR backed CPW fed notch filter. (b) DS-ESRRs without and with 60° rotations of the inner ring.

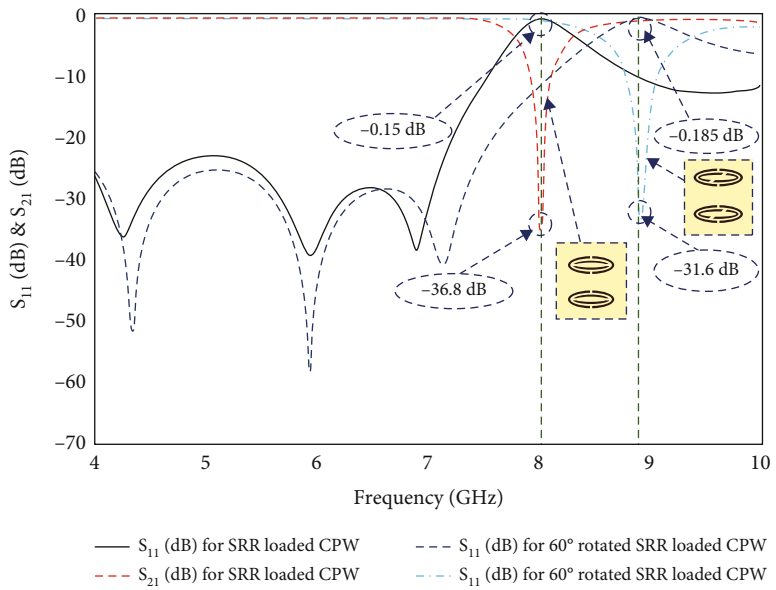

FIGURE 11: S-parameter plots of the proposed DS-ESRR without and with 60° rotation of inner ring loaded notch filter.

Neglecting the gap capacitance, equation (15) can be approximated as follows

$$f_0^{\text{DS-ESRR}} = \frac{1}{2\pi\sqrt{L_T^{DS}(\pi+x)\left[\left(a_{\text{avg}}+b_{\text{avg}}\right)R_cC_{\text{pul}}/16\right]}}. \quad (28)$$

Comparing equations (27) and (28), we can come up with the relation between the resonance frequency of DS-ESRR and that of the rotated DS-ESRR as follows

$$\frac{f_{r0}^{\text{DS-ESRR}}}{f_0^{\text{DS-ESRR}}} = \frac{2(\pi+x)}{\sqrt{(\pi+x)^2-\theta^2}}. \quad (29)$$

For the very small value of x, equation (29) can be further compressed as

$$\frac{f_{r0}^{\text{DS-ESRR}}}{f_0^{\text{DS-ESRR}}} = \frac{2\pi}{\sqrt{\pi^2-\theta^2}} \quad (30)$$

2.4. Mathematical Analysis Based on Material Properties. The most commonly used conversion model for S-parameters to dielectric properties is the NRW (Nicolson-Ross-Weir) method [11–13], as it gives information on both the electric and magnetic properties of a material. Figure 6 shows the schematic of the necessary and essential boundary conditions set-up in the HFSS EM-simulator for the edge-coupled elliptical split ring resonator (E-SRR) here to extract its S-parameters to estimate its effective relative permeability,

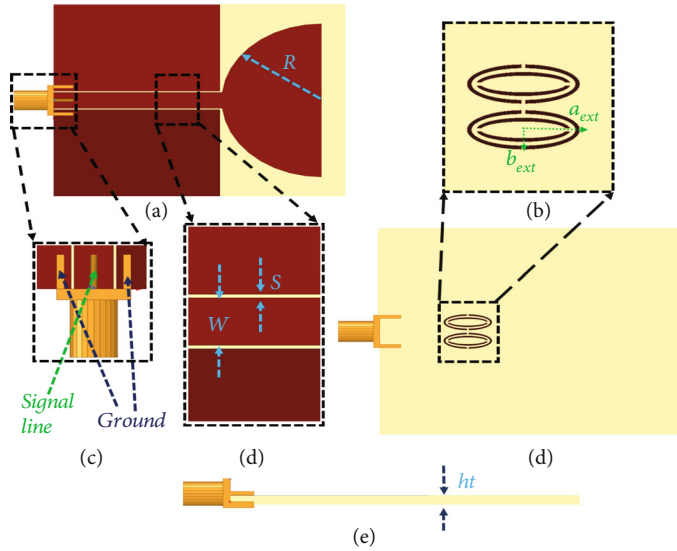

FIGURE 12: (a) Top view of the schematic of the proposed UWB filtenna. (b) Close view of the DS-ESRR at 8 GHz. (c) Close view of the SMA connector with the CPW. (d) Close view of the CPW feed. (e) Back view of the proposed filtenna. (f) Side view of the filtenna.

effective relative permittivity, effective refractive index, and effective impedance of the resonator unit.

The complex permittivity extraction technique, called NRW, was developed by Nicolson, Ross, and Weir. The NRW provides a direct calculation of the dielectric properties [14, 15] with the help of transmission (T) and reflection (Γ) coefficients, which are extracted by using S-parameters and shown in Figures 7(a)–7(d). Fundamental mode S-parameter relationships are then used to solve for permeability and permittivity, $\mu(\omega)$ and $\epsilon(\omega)$, respectively, as a function of the angular frequency ω.

2.5. Empirical Relationship Modelling Using Nonlinear Curve-Fitting Tool. In this section, different empirical relations have been proposed for the design of the double-split ring resonator (DS-SRR) and rotational. Depending upon the different electrical parameters of the structure, the effect on the resonance frequency of the SRR structure has been modelled as a customized empirical nonlinear relationship. Two cases are taken into consideration here. In the first case, the semimajor and semiminor axes of the outer elliptical ring are sequentially varied to estimate the effects on the resonating frequency. Due to the nonlinear variation of semimajor, different semiminor axis values have been correlated and returned to the resonance frequencies of the DS-ESRR. From the parametric data taken from the simulation environment, due to the nonconvex nature and some nonlinear dependency of column basis vectors, linear regression becomes inefficient in correlating different basis values. Therefore, a customized curve-fitting tool is used to achieve the estimation of the optimum correlation between basis data and the final empirical equation using the MATLAB computational platform.

The abovementioned double-split elliptical SRR (DS-ESRR) can be nonlinearly mapped into the jointly distributed vector span of the semimajor axis (a_{ext}) and semiminor axis (b_{ext}). The cross-correlated vector basis can be effectively mapped into the resonating frequency of the SRR through the Loess regression process by obtaining a multivariate Gaussian distribution. The multivariate Gaussian distribution can be expressed as

$$p(x|\mu,\Sigma) = \frac{1}{(2\pi)^{p+q/2}|\Sigma|^{0.5}} \times \exp \cdot \left\{ -\frac{1}{2} \begin{pmatrix} x_1-\mu_1 \\ x_2-\mu_2 \end{pmatrix}^T \begin{bmatrix} \Sigma_{11} & \Sigma_{12} \\ \Sigma_{21} & \Sigma_{22} \end{bmatrix}^{-1} \begin{pmatrix} x_1-\mu_1 \\ x_2-\mu_2 \end{pmatrix} \right\}, \tag{31}$$

where $\mu = \begin{pmatrix} 1.44 \\ 0.31 \end{pmatrix}$ and $\Sigma_{11} = 4.25$, $\Sigma_{22} = 2.5$, Σ_{12}, and $\Sigma_{21} = 0$.

Based on the above distribution, the jointly distributed X_1 and X_2 vectors have been mapped to the semimajor axis (a_{ext}) and semiminor axis (b_{ext}). The respective contour plots and residuals have been mentioned in Figure 8 for each basis vector.

For example, the resonance frequency of the rotational double-split elliptical SRR (DS-ESRR) can be again nonlinearly mapped into the jointly distributed vector span of the semimajor axis (a_{ext}) and relative angular orientation (θ) of the inner splits. The cross-correlated vector basis can be effectively mapped into the resonating frequency of the SRR through the Loess regression process by obtaining a multivariate Gaussian distribution. The multivariate Gaussian distribution can be expressed this time as

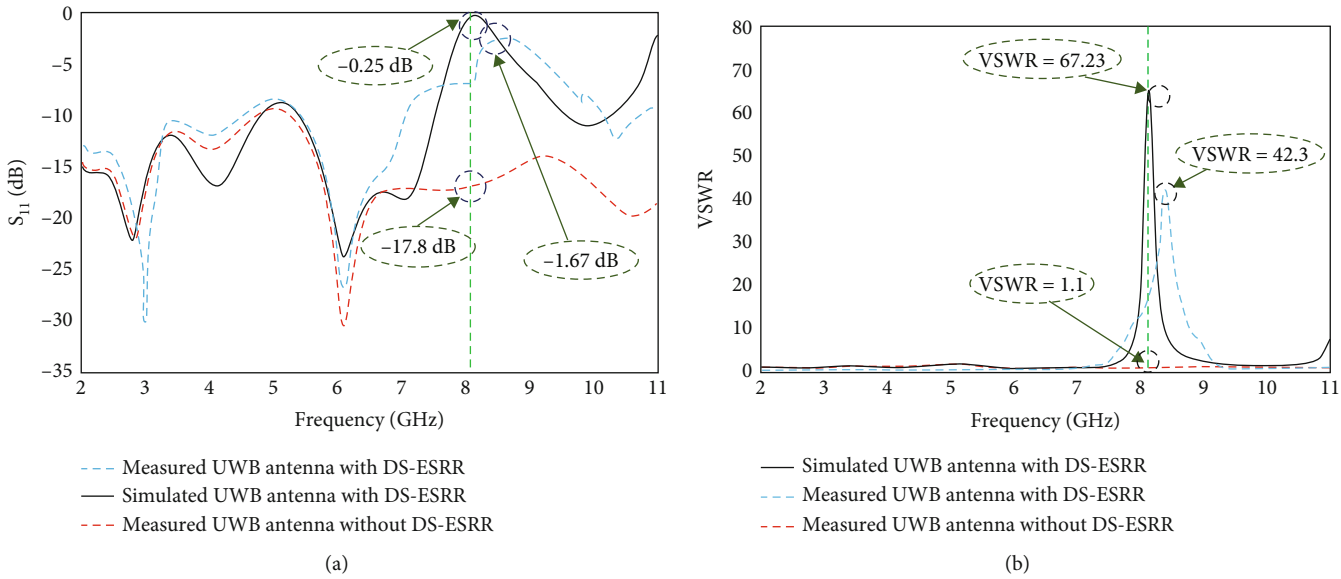

FIGURE 13: (a) Comparison between the simulated and measured S_{11} (dB) plots of the proposed UWB filtenna. (b) Comparison between the simulated and measured VSWR plots of the proposed UWB filtenna.

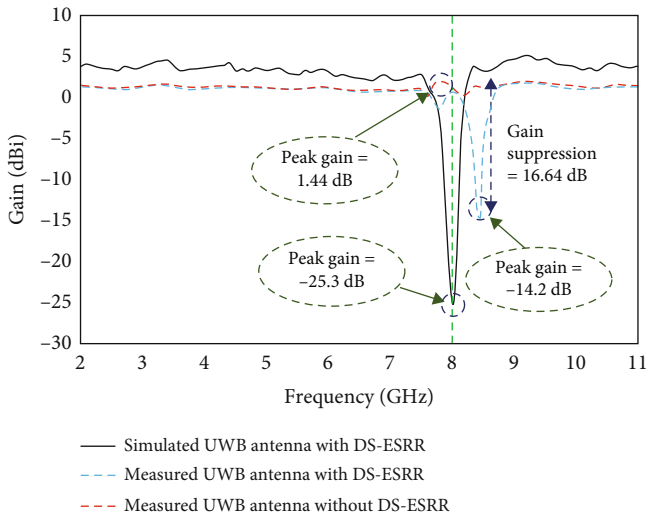

FIGURE 14: Comparison between the simulated and measured peak gain plots of the proposed UWB filtenna.

$$p(x|\mu,\Sigma) = \frac{1}{(2\pi)^{p+q/2}|\Sigma|^{0.5}} \times \exp \cdot \left\{ -\frac{1}{2} \begin{pmatrix} x_1 - \mu_1 \\ x_2 - \mu_2 \end{pmatrix}^T \begin{bmatrix} \Sigma_{11} & \Sigma_{12} \\ \Sigma_{21} & \Sigma_{22} \end{bmatrix}^{-1} \begin{pmatrix} x_1 - \mu_1 \\ x_2 - \mu_2 \end{pmatrix} \right\}, \quad (32)$$

where $\mu = \begin{pmatrix} 4.25 \\ 45 \end{pmatrix}$ and $\Sigma_{11} = 1.44$, $\Sigma_{22} = 28.87$, Σ_{12}, and $\Sigma_{21} = 0$.

Based on the above distribution, the jointly or bivariately distributed X_1 and X_2 vectors have been mapped to the semimajor axis (a_{ext}) and relative angular orientation (θ) of the inner splits. The respective contour plots and residuals have been mentioned in Figure 9 for each basis vector.

3. Results and Discussions

3.1. Filter Realization with Strong Notch. Figure 10(a) shows the schematic diagram of the DS-ESRR-loaded CPW-fed notch filter. The DS-ESRR is designed for 8 GHz on the top of a Rogers RT-5870 substrate having a relative permittivity of $\varepsilon_r = 2.33$ and a dielectric height of $h_t = 1.575$ mm, backed by a 50-ohm coplanar waveguide (CPW) transmission line. The strip line width is $W = 5$ mm, and the slot width is $S = 0.5$ mm. Here, the semimajor and minor axes of the ellipse are taken as $a_{ext} = 5.5$ mm and $b_{ext} = 2.3$ mm. Figure 11 shows the schematic of the DS-ESRRs with 60° rotation and without the rotation of the inner ring. The S_{11} and S_{21} plots are shown in Figure 10, where initially we had $S_{11} = -36.8$ dB and $S_{21} = -0.15$ dB at 8 GHz, but after rotating the inner ring relatively by 60°, the resonance frequency of the SRR got shifted to 9 GHz for the rotational effect, and $S_{11} = -31.6$ dB and S_{21} reached up to -0.185 dB at the notch frequency. This implies very strong and highly notching characteristics of the DS-ESRR.

3.2. Proposed UWB Filtenna. The proposed DS-ESRR of 8 GHz is integrated with the 50 ohm-CPW-fed transmission line, where the CPW feed line is extended to a semicircular ultrawideband monopole patch antenna having a radius of $R = 12.5$ mm on the same substrate (Rogers 5870) as the filter. Figure 12 reveals the detailed schematic view of the proposed filtenna structure, and Table 2 shows the design parameters in detail.

Table 3: Comparative study between recent works and present works.

Ref.	Antenna type	Antenna size	Frequency range	Gain	Year of publication
[17]	Compact, single-layered substrate integrated waveguide filtenna with parasitic patch	$46 \times 37\ mm^2$	2.21 & 2.95 GHz	6.3 dBi	2019
[18]	Circular monopole antenna an inverted L-shaped stub attached to the microstrip feed line	$35 \times 44\ mm^2$	3.4-3.8 GHz	3.5 and 3.15 dBi	2021
[19]	SRR defected ground structure filtenna	$20 \times 19.5 \times 1.524\ mm^3$	5.9 GHz	—	2021
[20]	Coplanar waveguide-fed monopole antenna is comprised of a rectangular-shaped structure with a slot and a Y-shaped radiator	$10 \times 15 \times 0.254\ mm^3$	3–14.55 GHz	3.2 dBi	2023
	Present work	$10.2 \times 12.5 \times 0.787\ mm^3$	3.1-10.6 GHz	4.25 dBi	2023

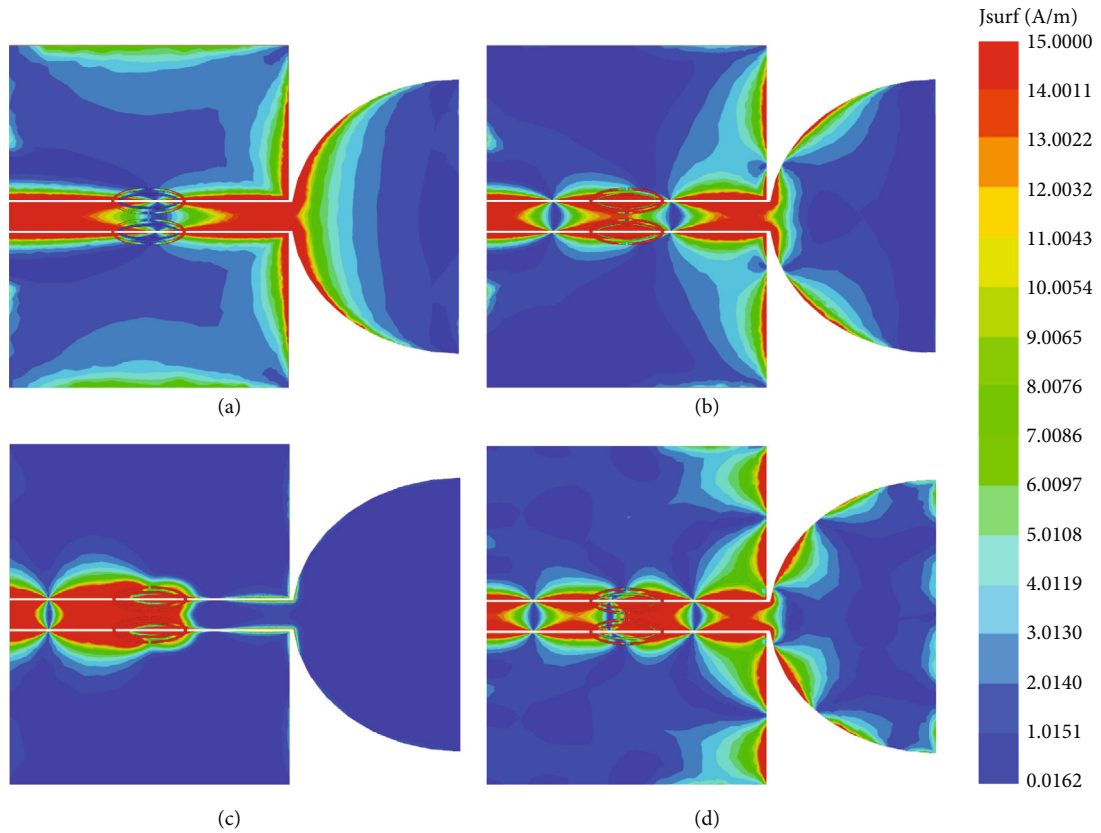

Figure 15: Surface current density visualization of the proposed UWB filtenna at (a) 3.1 GHz, (b) 6.5 GHz, (c) 8.1 GHz, and (d) 10 GHz.

Figures 13(a), 13(b), and 14 show the S_{11} (dB), VSWR, and peak gain stability plots of the simulated and measured results of the proposed filtenna, respectively. As shown in Figure 13(a), the S_{11} (dB) for the simulated design with the DS-ESRR reaches -0.25 dB at 8 GHz, where the measured data shifted to 8.4 GHz without and with the DS-ESRR are -17.8 dB and -1.67 dB, respectively. To realize the effective characterization of the DS-ESRR-loaded UWB antenna, circuit modelling has been explained using CPW-fed architecture in [16].

Figure 13(b) reveals that the VSWR for the simulated design with the DS-ESRR is 67.23 at 8 GHz, whereas the measured VSWR at 8.4 GHz without and with the DS-ESRR are 1.1 and 42.3, respectively. From Figure 14, it is revealed that the gain stability for the simulated design with the DS-ESRR reaches 3.6 dBi at 8 GHz, whereas the measured gain at the shifted frequency of 8.4 GHz without and with the DS-ESRR is 1.44 dBi and -14.2 dBi, respectively. It implies that the DS-ESRR provides a gain suppression of 16.64 dB, which

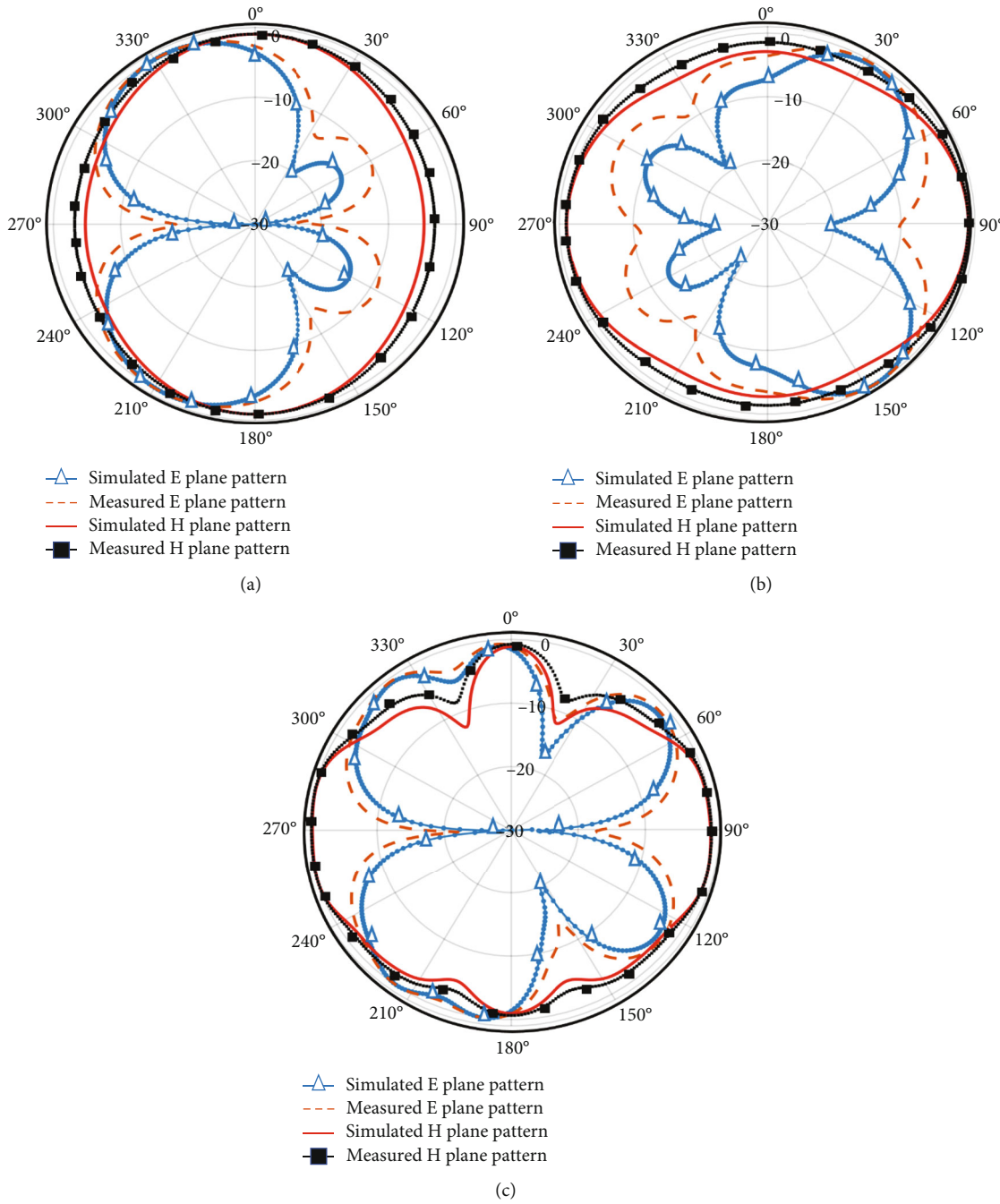

Figure 16: E-plane and H-plane 2D radiation patterns of the proposed UWB filtenna at (a) 3.1 GHz, (b) 6.5 GHz, and (c) 10 GHz.

is very convincing. A comparative table based on recent works and proposed concepts is being displayed in Table 3.

Figure 15 presents a visualization of the current density of the antenna at different frequencies within its bandwidth. As revealed from Figures 15(a), 15(b), and 15(d) for the current travelling from the CPW feed to the semicircular monopole patch, the pair of the DS-ESRR seems to be transparent, but at 8.1 GHz, the SRRs resonate and show very strong stop-band characteristics. Figure 16 reveals the E-plane and H-plane 2D radiation patterns of the proposed antenna. Figures 16(a)–16(c) show the gain patterns at 3.1 GHz, 6.5 GHz, and 10 GHz, respectively.

Figures 17(a) and 17(c) are the top and bottom views of the fabricated antenna, respectively. Figures 12(b) and 12(d) are the snaps from the VNA while measuring the S-parameter and VSWR plot, respectively. Figures 18(a)–18(c) show some of the snaps of the vector network analyzer (VNA) while measuring the gain patterns of the fabricated ultrawideband filtenna.

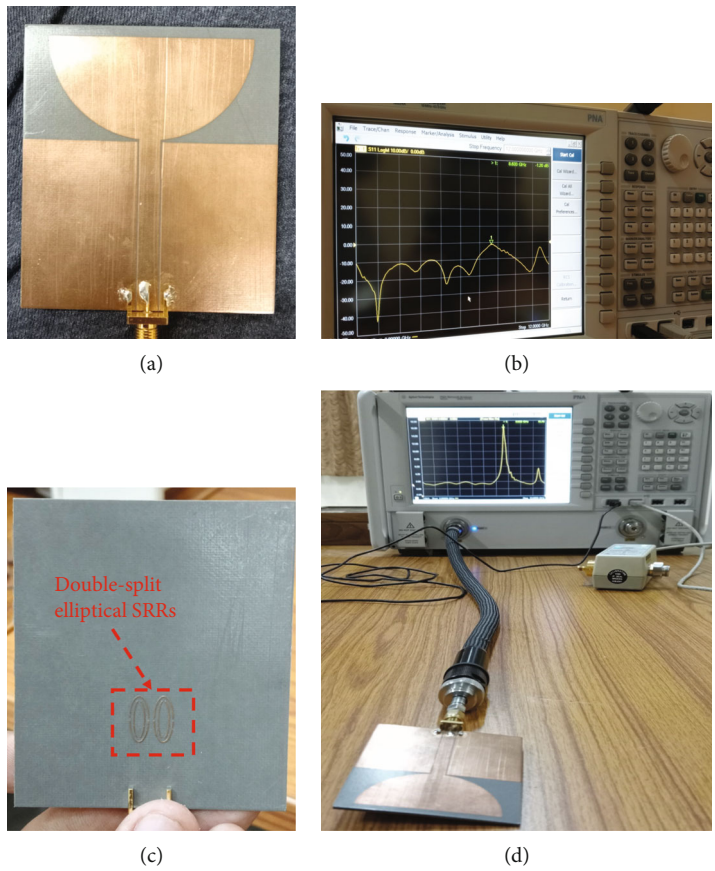

FIGURE 17: (a) Top view of the fabricated UWB filtenna structure. (b) S-parameter measurement of the antenna using VNA. (c) Top view of the fabricated UWB filtenna structure. (d) VSWR measurement of the antenna using VNA.

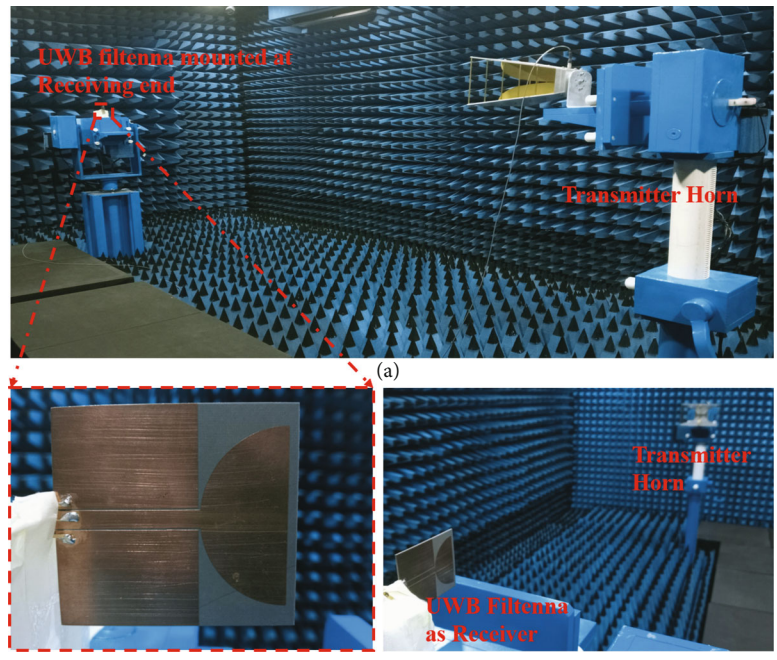

FIGURE 18: (a) Gain pattern measurement in an anechoic chamber facility. (b) Close view of the fabricated UWB filtenna at the receiving end.

4. Conclusion

The theoretical analysis of elliptical SRR and double-split elliptical SRR (ESRR) is proposed here in this manuscript. The stop-band characteristics of the double-split elliptical SRR (DS-ESRR) are presented with the help of an UWB filtenna structure in detail. The proposed idea is very simple and can be scaled to any other futuristic application.

Data Availability

Data may be available upon request.

Conflicts of Interest

The authors declare that they have no conflicts of interest.

References

[1] J. Zhou, T. Koschny, M. Kafesaki, E. N. Economou, J. B. Pendry, and C. M. Soukoulis, "Saturation of the magnetic response of split-ring resonators at optical frequencies," *Physical Review Letters*, vol. 95, no. 22, article 223902, 2005.

[2] R. Marqués, J. Martel, F. Mesa, and F. Medina, "Left-handed-media simulation and transmission of EM waves in subwavelength split-ring-resonator-loaded metallic waveguides," *Physical Review Letters*, vol. 89, no. 18, article 183901, 2002.

[3] F. Martın, J. Bonache, F. A. Falcone, M. Sorolla, and R. Marqués, "Split ring resonator-based left-handed coplanar waveguide," *Applied Physics Letters*, vol. 83, no. 22, pp. 4652–4654, 2003.

[4] A. B. Movchan and S. Guenneau, "Split-ring resonators and localized modes," *Physical Review B.*, vol. 70, no. 12, p. 125116, 2004.

[5] X. C. Zhang, Z. Y. Yu, and J. Xu, "Novel band-pass substrate integrated waveguide (SIW) filter based on complementary split ring resonators (CSRRs)," *Progress In Electromagnetics Research*, vol. 72, pp. 39–46, 2007.

[6] J. Y. Siddiqui, C. Saha, and Y. M. M. Antar, "Compact SRR loaded UWB circular monopole antenna with frequency notch characteristics," *in IEEE Transactions on Antennas and Propagation*, vol. 62, no. 8, pp. 4015–4020, 2014.

[7] L. A. Shaik, C. Saha, Y. M. M. Antar, and J. Y. Siddiqui, "An antenna advance for cognitive radio: introducing a multilayered split ring resonator-loaded printed ultrawideband antenna with multifunctional characteristics," *IEEE Antennas and Propagation Magazine*, vol. 60, no. 2, pp. 20–33, 2018.

[8] Y. Wang, T. Huang, D. Ma, P. Shen, J. Hu, and W. Wu, "Ultra-wideband (UWB) monopole antenna with dual notched bands by combining electromagnetic-bandgap (EBG) and slot structures," in *2019 IEEE MTT-S International Microwave Biomedical Conference (IMBioC)*, pp. 1–3, Nanjing, China, 2019.

[9] C. Saha, J. Y. Siddiqui, A. P. Freundorfer, L. A. Shaik, and Y. M. M. Antar, "Active reconfigurable ultra-wideband antenna with complementary frequency notched and narrowband response," *IEEE Access*, vol. 8, pp. 100802–100809, 2020.

[10] S. Basu, S. Pahadsingh, and S. Sahu, "Compact elliptical slotted antenna with multi bands notched for UWB applications," in *2021 IEEE 2nd International Conference on Applied Electromagnetics, Signal Processing, & Communication (AESPC)*, Bhubaneswar, India, 2021.

[11] M. B. Villarino, "Ramanujan's perimeter of an ellipse," 2005, https://arxiv.org/abs/0506384.

[12] K.-Z. Hu, M.-C. Tang, D. Li, W. Yang, and M. Li, "Design of compact, single-layered substrate integrated waveguide filtenna with parasitic patch," *IEEE Transactions on Antennas and Propagation*, vol. 68, no. 2, pp. 1134–1139, 2020.

[13] T. H. Al-Arajee and K. H. Sayidmarie, "A rectangular monopole filtenna with U-shaped slot for 5G applications," *International Journal of Microwave & Optical Technology*, vol. 1152, no. 1, p. 012011, 2021.

[14] N. Gupta, P. Bhardwaj, and S. Balhara, "Designing of defected ground structure patch antenna for vehicular safety applications at 5.9 GHz," *Wireless Personal Communications*, vol. 121, no. 1, pp. 95–106, 2021.

[15] S. N. Rizvi, W. A. Raza, D. C. Awan, N. Hussain, S. G. Park, and N. Kim, "A compact size antenna for extended UWB with WLAN notch band stub," *Applied Sciences*, vol. 13, no. 7, p. 4271, 2023.

[16] C. Saha, J. Y. Siddiqui, and Y. M. M. Antar, *Multifunctional Ultrawideband Antennas: Trends, Techniques and Applications*, CRC Press, 1st edition, 2019.

[17] N. Mishra, A. Chandra, D. K. Choudhary, and R. Kumar, "CRLH-TL based dual-band miniaturized antenna for microwave communication," in *2022 IEEE Conference on Interdisciplinary Approaches in Technology and Management for Social Innovation (IATMSI)*, Gwalior, India, 2022.

[18] D. K. Choudhary, N. Mishra, P. K. Singh, and A. Sharma, "Miniaturized power divider with triple-band filtering response using coupled line," *IEEE Access*, vol. 11, pp. 27602–27608, 2023.

[19] D. K. Choudhary and R. K. Chaudhary, "Compact filtering antenna using asymmetric CPW-fed based CRLH structure," *AEU-International Journal of Electronics and Communications*, vol. 126, article 153462, 2020.

[20] D. K. Choudhary and R. K. Chaudhary, "Compact D-CRLH structure for filtering power divider," *Progress In Electromagnetics Research Letters*, vol. 94, pp. 93–101, 2020.